Size-Dependent Chromaticity in YBO_3:Eu Nanocrystals: Correlation with Microstructure and Site Symmetry

Zhenggui Wei, Lingdong Sun,* Chunsheng Liao, Jialu Yin, Xiaocheng Jiang, and Chunhua Yan*

State Key Laboratory of Rare Earth Materials Chemistry and Applications, PKU-HKU Joint Laboratory on Rare Earth Materials and Bioinorganic Chemistry, Peking University, Beijing 100871, China

Shaozhe Lü

Open Laboratory of Excited States, Chinese Academy of Sciences, Changchun 130021, China

Received: April 18, 2002; In Final Form: July 11, 2002

Pure hexagonal-phased $Y_{1-x}BO_3$:Eu_x ($x = 0-0.30$) nanocrystals with different particle sizes were prepared by a facile sol−gel pyrolysis process, and their photoluminescence spectra evidently showed a size-dependent characteristic because the ratio of the red emission transition ($^5D_0 \rightarrow {}^7F_2$) to the orange emission transition ($^5D_0 \rightarrow {}^7F_1$) (R/O) was much higher in the smaller particles. Both XRD patterns and IR spectra demonstrated that the lattices of YBO_3:Eu nanocrystals were distorted and that as the particle size became smaller, the lattices became more distorted. Studies on the charge transfer (CT) bands indicated that Eu^{3+} ions can be excited preferentially by different excitation sources in both the bulk and the nanocrystals, suggesting that at least two different types of intrinsic luminescent sites, site **1** and site **2**, coexist in YBO_3:Eu. Site-selective excitation spectra also revealed that a particular site, site **3**, existed concurrently in the nanocrystals. Site **2**, the site with relatively inferior symmetry of the intrinsic sites, was identified to be of C_1 symmetry. Meanwhile, for the nanosized samples, Eu^{3+} ions exhibited enhanced R/O values in both sites **2** and **3**, which might be ascribed to the distorted lattices, and thus displayed the observed superior color chromaticity. A pronounced energy transfer between site **2** and site **3** in the nanocrystals was also observed while Eu^{3+} concentration was increased to the quenching concentration, which indicated that site **3** may be a disordered surface site surrounding the interior sites.

1. Introduction

To meet the demands of plasma display panels (PDPs) and a new generation of Hg-free fluorescent lamps, phosphors with a high quantum efficiency and high vacuum ultraviolet (VUV) absorption are required.[1,2] Much attention has been paid to the phosphors with quantum cutting effect for their two-photon visible emission under VUV excitation.[3,4] However, even including this quantum cutting effect, the efficiency and absorption of these phosphors are still not satisfying, for example, $LiGdF_4$:Eu, for which overall quantum efficiency is only 32%, despite that its downcoversion efficiency approaches 200%.[5]

Until recently, as far as quantum efficiency and VUV absorption are concerned, rare earth (RE) orthoborate, YBO_3:Eu, is still one of the best red phosphors, which performs high VUV transparency and exceptional optical damage threshold.[6] However, all of this excellence does not make YBO_3:Eu a desired VUV luminescent material because of its chromaticity problem. The characteristic emission of YBO_3:Eu is composed of almost equal contributions from $^5D_0-{}^7F_1$ and $^5D_0-{}^7F_2$ transitions, which gives rise to an orange-red emission instead of a red one, whereas concentration of the main emission in the $^5D_0-{}^7F_2$ is required in terms of application. Considering that the $^5D_0-{}^7F_2$ transition is hypersensitive to the symmetry of the crystal field and will be relatively strong if the symmetry of the crystal field is relatively low, we attempt to reduce the symmetry of the crystal field to solve the chromaticity drawback of YBO_3:Eu, in terms of increasing the contribution of $^5D_0-{}^7F_2$ transition. Simple and effective as it may seem to lower the symmetry of the crystal field by changing the structure of the borate ions in YBO_3:Eu, studies showed that the wonderful VUV absorption of referred rare earth borate relies much on the hexagonal vaterite-type structure,[7] thus making it harmful for us to adjust the borate group structurally. With respect to this, nanosized YBO_3:Eu was fabricated within a low crystal field symmetry, while maintaining the orthoborate structure, thus realizing the improvements of both chromaticity and fluorescence yield.[8]

The microstructural properties of nanosized materials have been extensively studied and discussed in previous reports and reviews. It is generally considered that the degree of disorder in the nanoparticles is relatively high, thereby a lower crystal field symmetry might be induced in such materials.[9−14] Many efforts have been devoted to the site symmetry determination of YBO_3:Eu; however, there are still considerable controversies about the local Eu^{3+} symmetry. For YBO_3:Eu^{3+}, Holsä[15] reported two types of Eu^{3+} sites with D_{3d} and T symmetry, and Chadeyron et al.[16] proposed two intrinsic sites of C_3 symmetry, while other authors regarded the local symmetry of YBO_3:Eu as D_3 and D_{3d},[17] three D_3 sites,[18] a unique C_1 site,[6] or D_3 and C_3[19]. In this paper, we present detailed studies on the micro-

* To whom correspondence should be addressed. E-mail: chyan@chem.pku.edu.cn.

10.1021/jp025967z CCC: $22.00
Published on Web 09/20/2002

structure and the site symmetry, the size dependence of chromaticity, and their correlation within the YBO_3:Eu nanocrystals.

Moreover, we introduce a facile sol−gel pyrolysis process for preparing YBO_3:Eu nanocrystals in this paper. YBO_3:Eu is apt to form highly agglomerated particles; therefore, although there are various fabrication processes of bulk YBO_3:Eu, such as solid-state reaction,[6] coprecipitation,[20] microwave heating,[21] spray pyrolysis,[22] and sol−gel method,[20] only a few reports were presented on the synthesis of YBO_3:Eu nanocrystals. Recently, Lou et al. prepared 40−60 nm YBO_3:Eu waveguide film through a sol−gel route,[23] starting from the preparation of boron yttrium and boron europium heterometallic alkoxides within a humidity controllable system. Zhang et al. synthesized 40 nm YBO_3:Eu nanocrystals using a different sol−gel method, whereas it is difficult to obtain a pure hexagonal-phase nanosized YBO_3:Eu at low calcination temperature (below 800 °C).[19] In this investigation, we have employed a precursor pyrolysis method using boric acid, yttrium, and europium−EDTA (ethylenediaminetetraacetic) complexes. The salient advantage of this fabrication is that pure hexagonal-phased YBO_3:Eu with high luminescence intensity and superior chromaticity can be obtained at low annealing temperature.

2. Experimental Section

2.1. Nanocrystal Synthesis. Appropriate amounts of $Y(NO_3)_3$, $Eu(NO_3)_3$, H_3BO_3, and $(NH_4)_2$−EDTA aqueous solutions were mixed together and kept stirring until a homogeneous solution was formed. The final pH was controlled as 6−7. By slow evaporation of the solvent, the complex precursors were obtained and dried at 80 °C under a vacuum for hours. Aliquots of the precursors were calcined at 650 °C for 100 min in oxygen, at 700 and 900 °C for 5 h in air to obtain nanosized YBO_3:Eu, and at 1100 °C for 5 h in air to obtain submicron-sized samples. These samples are denoted as **a**, **b**, **c**, and **d** series, respectively, in the following description. Because boric acid−EDTA complex has similar properties to yttrium− and europium−EDTA complexes, its formation might contribute to the avoidance of aggregation. Previously, it was neglected that boric acid can form a complex by reacting with the molecules that have two or more carboxyl (or hydroxyl) groups,[24] and to our knowledge, no one has yet utilized boric acid−EDTA complex as a precursor to synthesize nanosized borate materials.

For comparison, the bulk YBO_3:Eu was obtained by direct solid-state reaction from the mixture of Y_2O_3, Eu_2O_3, and H_3BO_3 at 1100 °C for 5 h in air.

2.2. Characterization. X-ray diffraction (XRD) studies were carried out on a Rigaku D/max-2000 X-ray powder diffractometer using Cu Kα (λ = 1.5405 Å) radiation. TEM images were taken on a Hitachi H-8000 NAR transmission electron microscope under a working voltage of 300 kV. The FTIR spectra were measured on a Nicolet Magna-IR 750. Fluorescence spectra were recorded on a Hitachi F-4500 spectrophotometer at room temperature. Brightness and CIE (Commission International del′Eclairge) color coordinates were calculated by integrating emission counts from a PR650 photomultiplier tube detector. Thermogravimetric−differential thermal analysis (TG−DTA) was investigated by using a Du Pont 2100 thermal analyzer in air. High-resolution fluorescence emission spectra and emission decay curves were measured at room temperature using a SPEX1403 double-grating monochromator and a R955 photomultiplier under 266 nm excitation provided by a frequency-quadrupled YAG:Nd laser. The site-selective excitation was performed by the same set of instruments with a rhodamine 6G laser pumped by the YAG:Nd laser.

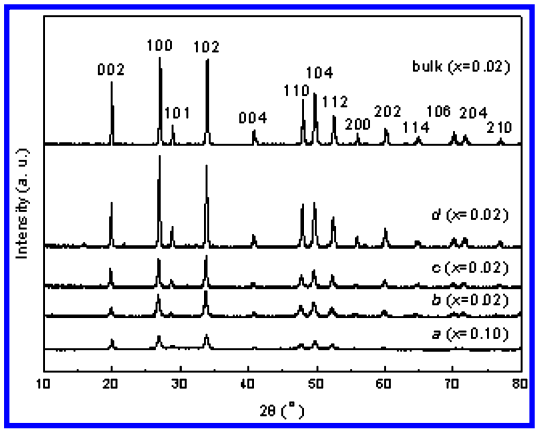

Figure 1. XRD patterns of $Y_{1-x}BO_3$:Eu_x samples. Complex precursors are decomposed at (a) 650 °C for 100 min and (b) 700, (c) 900, and (d) 1100 °C for 5 h. Bulk sample is obtained by direct solid-state reaction at 1100 °C for 5 h.

3. Results and Discussion

3.1. Microstructure Character of YBO_3:Eu Nanocrystals: XRD, TEM, and FTIR Studies. Figure 1 shows the XRD patterns of YBO_3:Eu samples, in which all of the peaks could be indexed to the hexagonal phase of YBO_3 with vaterite-type structure and no excessive traces of rare earth oxide were observed. By applying Scherrer formula to the full width at half-maximum of the diffraction peaks, we could calculate the mean particle size of $Y_{1-x}BO_3$:Eu_x as 19.5, 40.8, and 88.6 nm for **a**, **b**, and **c** samples with x = 0.02, respectively. Obviously, the sizes of YBO_3:Eu samples increased with annealing temperature and time. The least-squares refined crystallographic unit cell parameters were obtained by using the software "LAPOD",[25] as listed in Table 1. The values of all samples are roughly matched with YBO_3 standard values given in JCPDS (No. 16-277). An increscent trend of cell volume values and a decrescent trend of c/a values could be clearly observed as the particle size decreased.

To verify the main cause of cell parameter increase, we analyzed the **c** samples with different Eu^{3+} doping concentrations. The cell parameters of these samples were calculated from XRD patterns and listed in Table 1. As expected, because of the larger ionic radius of Eu^{3+} in comparison with Y^{3+}, doping Eu^{3+} into YBO_3 lattice also leads to a cell-parameter increase. However, unlike a decrescent trend of c/a values observed as the particle size decreased, the c/a values of all **c** samples were almost equal to each other and were around 2.325. The above phenomenon can be well interpreted if we take the c/a value as a measure of the lattice distortion in the YBO_3:Eu, preliminarily considering that the lattices are more distorted in the nanocrystals than in the bulk and that with smaller particle size the lattices become more distorted.

The TEM image of sample **b** is shown in Figure 2. It revealed that the YBO_3:Eu nanocrystals were spherelike particles with almost no amorphous constituents. The grain sizes are distributed in the range of 30−50 nm, which is consistent with the mean particle size deduced from XRD. The electron diffraction pattern shown in the inset of Figure 2 further confirmed the indexed hexagonal structure.

Figure 3 shows the FTIR spectra of $Y_{1-x}BO_3$:Eu_x samples **b** and **c** with x = 0.02 and **d** samples with different doping concentration. The IR absorption peaks between 800 and 1200

TABLE 1: Least-Squares Refined Unit Cell Parameters for $Y_{1-x}BO_3:Eu_x$ Bulk and Nanocrystalline Samples

sample[a]	*a* (Å)	*c* (Å)	*c*/*a*	cell volume (Å^3)
JCPDS std no. 16-277	3.778	8.81	2.332	108.90
bulk ($x = 0.02$)	3.7806 ± 0.0014	8.8214 ± 0.0036	2.3333 ± 0.0013	109.19 ± 0.008
a ($x = 0.10$)	3.8072 ± 0.0038	8.8168 ± 0.0093	2.3158 ± 0.0034	110.68 ± 0.199
b ($x = 0.02$)	3.8021 ± 0.0036	8.8340 ± 0.0089	2.3235 ± 0.0032	110.59 ± 0.190
c ($x = 0.02$)	3.7980 ± 0.0042	8.8276 ± 0.0104	2.3242 ± 0.0037	110.28 ± 0.219
d ($x = 0.02$)	3.7839 ± 0.0017	8.8200 ± 0.0042	2.3309 ± 0.0015	109.37 ± 0.088
c ($x = 0.001$)	3.7840 ± 0.0007	8.8154 ± 0.0017	2.3292 ± 0.0006	109.36 ± 0.035
c ($x = 0.1$)	3.7989 ± 0.0012	8.8381 ± 0.0029	2.3265 ± 0.0010	110.46 ± 0.060
c ($x = 0.2$)	3.8091 ± 0.0014	8.8637 ± 0.0036	2.3270 ± 0.0013	111.38 ± 0.077
c ($x = 0.3$)	3.8307 ± 0.0010	8.9030 ± 0.0024	2.3241 ± 0.0009	113.14 ± 0.051

[a] Complex precursors are decomposed at 650 °C for 100 min for **a** and at 700 , 900, and 1100 °C for 5 h for **b**, **c**, and **d**, respectively. Bulk sample is obtained by direct solid-state reaction at 1100 °C for 5 h.

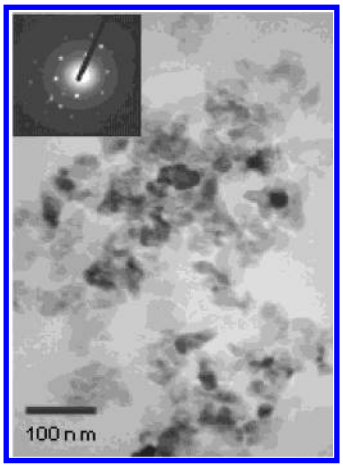

Figure 2. TEM image and electron diffraction of YBO_3:Eu nanocrystals prepared at 700 °C for 5 h.

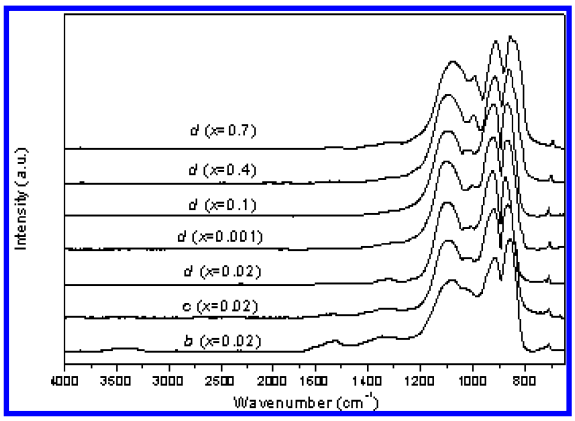

Figure 3. FTIR spectra of $Y_{1-x}BO_3:Eu_x$ samples. Samples **b**−**d** are denoted in the text and Figure 1.

cm^{-1} are typical for the polyborate group $B_3O_9^{9-}$.[6,26] The structure of $B_3O_9^{9-}$ is shown in Figure 4. According to the referenced IR assignments,[6,26,27] we consider the IR absorption peaks in the region of 800−950 cm^{-1} to be of ring stretch vibration modes (RS) and the peaks in the region of 950−1200 cm^{-1} to be of terminal stretch vibration modes (TS). The origins of the absorption peaks and their intensities were listed in Table 2. With the particle size decreasing, all absorption peaks red-shifted and the intensity ratio of RS to TS decreased. However, higher doping concentration only induced red shifts of IR absorption peaks without changing the intensity ratio of RS to TS. According to Hooke's law,[28] as the bond distances become longer, force constants become lower and IR absorption wavelength will be longer. Therefore, red-shifts of IR absorption indicate that longer B−O bond distances should exist for the samples with smaller particle size, as well as those with higher doping concentration.

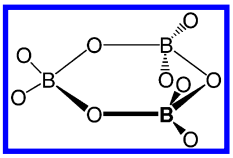

Figure 4. Structural sketch map of $B_3O_9^{9-}$ ion.

Meanwhile, the intensity of IR absorption relates to the content of the bonds that perform the relevant vibration mode. Therefore, we deduced that the number of the terminal O atoms should be fewer in the smaller particles and almost unaltered as the contents of Eu^{3+} ions varied. The deficiency of terminal O atoms should be responsible for the lattice distortion in the nanocrystals. Previous studies showed that, in addition to the limited coherence length of the nanocrystals, many bulk and surface defects existed as a consequence of the low-temperature synthesis and the high surface area of the crystallites.[29] These defects probably accounted for the deficiency of terminal O atoms in the nanocrystals.

3.2. Chromaticity and Brightness of YBO_3:Eu Nanocrystals. *3.2.1. Size-Dependent Chromaticity.* Figure 5 displays the emission spectra of YBO_3:Eu under 240 nm UV irradiation. All of them were normalized to their maximum. The spectra consist of sharp lines ranging from 580 to 720 nm, which are associated with the transitions from the excited $^5D_0$ level to ^7F_J ($J = 1, 2, 3, 4$) levels of Eu^{3+} activators,[30] of which the major emissions are centered at 591 nm ($^5D_0-^7F_1$) and 610 and 625 nm ($^5D_0-^7F_2$), well-corresponding to orange-red and red color, respectively. Although the major peak positions in the emission spectra are identical to each other, the intensity patterns are much different. For the bulk and submicron-sized samples, the $^5D_0-^7F_1$ transition is the most intense one.[22] But for the nanosized particles, the relative intensity of $^5D_0-^7F_2$ increased with decreasing particle size. It is obvious that with the particle size decreasing the red emission coming from $^5D_0-^7F_2$ increases, and as a result, a redder fluorescence in chromatic sense, that is, a superior chromaticity, can be obtained.

The intensity of the transitions between different *J* levels depends on the symmetry of the local environment of the Eu^{3+} activators and can be described in terms of Judd−Ofelt theory.[31] According to the selective rules, magnetic dipole transition is permitted and electric dipole transition is forbidden, but for some cases in which the local symmetry of the activators is without an inversion center, the parity forbiddance is partially permitted, such as Eu^{3+} ions occupying C_2 sites in Y_2O_3:Eu.[31] It is well-known that the relative intensity of $^5D_0-^7F_1$ and $^5D_0-^7F_2$ transitions depends strongly on the local symmetry of Eu^{3+} ions. Subsequently, when Eu^{3+} ions occupy the sites with inversion centers, the $^5D_0-^7F_1$ transition should be relatively strong, while

TABLE 2: Peak Positions and Intensities of FTIR Spectra for $Y_{1-x}BO_3:Eu_x$ Samples

sample		terminal stretch				ring stretch	
b ($x = 0.02$)	peak positions (cm^{-1})	1078		1028		916	860
	peak intensities	0.6356		0.5598		0.8354	1
c ($x = 0.02$)	peak positions (cm^{-1})	1086		1028	1008	920	869
	peak intensities	0.6922		0.5302	0.5272	0.9629	1
d ($x = 0.02$)	peak positions (cm^{-1})	1097		1032	1008	924	878
	peak intensities	0.7535		0.5	0.5123	1	0.9479
d ($x = 0.001$)	peak positions (cm^{-1})	1101			1003	924	870
	peak intensities	0.7914			0.5748	1	0.9745
d ($x = 0.1$)	peak positions (cm^{-1})	1093	1089	1027	1009	920	870
	peak intensities	0.7563	0.7568	0.585	0.5889	0.999	1
d ($x = 0.4$)	peak positions (cm^{-1})	1093			997	916	862
	peak intensities	0.7794			0.5973	0.9369	1
d ($x = 0.7$)	peak positions (cm^{-1})	1074			993	912	858
	peak intensities	0.7687			0.6471	0.9492	1

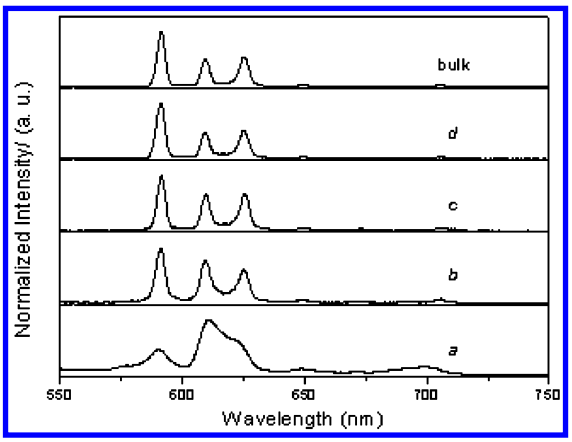

Figure 5. Emission spectra of YBO_3:Eu samples. Samples **a**−**d** and bulk are denoted in the text and Figure 1.

the $^5D_0-^7F_2$ transition is parity-forbidden and should be very weak. The abnormal luminescent behavior of the nanosized YBO_3:Eu must be correlated to the microstructure. As mentioned above, the distorted lattices and the terminal oxygen deficiencies in the nanosized YBO_3:Eu may increase the degree of disorder and lower the local symmetry of Eu^{3+} ions, and as a consequence, the transition probability of $^5D_0-^7F_2$ is increased and the visual color is improved.

3.2.2. Size-Dependent Quenching Concentration. The relationship between luminescence intensity and dopant content is shown in Figure 6. The dependence of $^5D_0-^7F_2$ and $^5D_0-^7F_1$ transitions on the activator concentration is identical for different sized YBO_3:Eu samples, but the quenching concentration varies. It is about 0.08 for the bulk YBO_3:Eu and increases to 0.15 and 0.20 for 88.6 and 40.8 nm samples, respectively. It is worth noting that quenching concentration increases with decreasing the particle size, as has been observed in other kinds of nanocrystals.[29,32] It is understandable that the concentration quenching effect is due to the possible nonradiative transfer between neighboring Eu^{3+} ions, which increases the mobility of the excited states within the host matrix and therefore increases the probability of nonradiative de-excitation via quenching centers (traps).[33,34] In nanosized materials, the deficiency of the traps due to the limited primitive cells per particle results in the fact that the traps distribute randomly with a considerable fluctuation between particles; there must be more traps in some of the particles while fewer traps in others.[12,33] Resonance energy transfer only occurs within one particle because of the hindrance by the particle boundary. Therefore, with increasing the concentration of luminescent centers, quenching occurs first in particles containing more traps, while

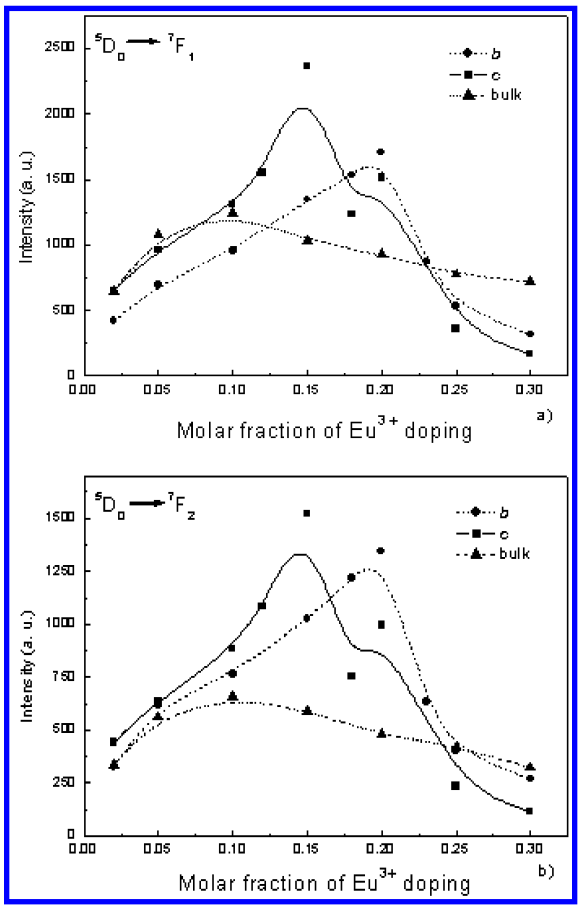

Figure 6. Quenching concentration of YBO_3:Eu for samples **b** and **c** and bulk obtained by monitoring the emissions of (a) $^5D_0-^7F_1$ (at 591 nm) and (b) $^5D_0-^7F_2$ (at 610 nm).

those particles with few or no traps quench only at high concentration or do not quench at all. Therefore, quenching occurs at higher Eu concentration in smaller particles. The quantum efficiency is another important factor to be studied, and the detailed investigation is in progress.

3.2.3. Color Coordinates (x, y) and Relative Brightness. Color coordinates (x, y) and relative brightness of $Y_{0.9}BO_3:Eu_{0.1}$ were presented in Table 3. Previous studies showed that the luminescence intensity of YBO_3:Eu was influenced by the synthesis method. The YBO_3:Eu obtained by the sol−gel method appeared to have a higher luminescence intensity in comparison with that prepared by the solid-state reaction.[20] Our work was similar to those results, as the brightness of sample **d** is 1.44 times as high as that of the bulk prepared by the solid-state reaction

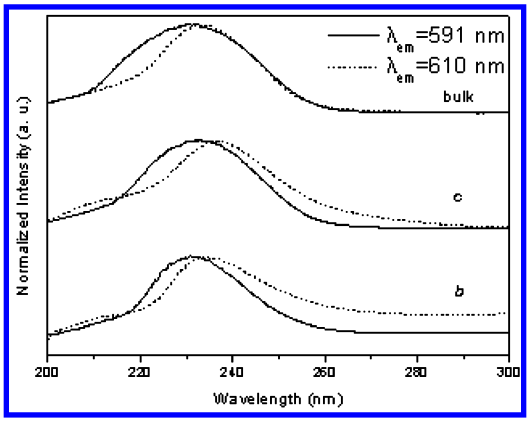

Figure 7. Excitation spectra of YBO_3:Eu for samples **b** and **c** and bulk obtained by monitoring the emissions of $^5D_0 \rightarrow {}^7F_1$ (at 591 nm) and $^5D_0 \rightarrow {}^7F_2$ (at 610 nm).

TABLE 3: Color Coordinates (*x*, *y*) and Relative Brightness of $Y_{0.9}BO_3:Eu_{0.1}$ Samples

	CIE coordinate		
sample	*x*	*y*	relative brightness
bulk	0.638	0.355	1
a	0.661	0.330	0.182
b	0.646	0.346	0.688
c	0.645	0.348	1.06
d	0.639	0.359	1.44

(Table 3). Moreover, the luminescent intensities of $Y_{1-x}BO_3$:Eu_x nanocrystals at their quenching concentrations ($x = 0.15$ and 0.20 for 88.6 and 40.8 nm YBO_3:Eu nanoparticles, respectively) were higher than that of the bulk ($x = 0.08$) (Figure 6), which suggested potential applications of the nanocrystals. From Table 3, we can also find that the chromaticity of the nanocrystals is better than that of the bulk and as the particle size gets smaller, the chromaticity gets better. The magnitudes of the color coordinates (*x*, *y*) and relative brightness were satisfactorily coincident with the emission spectrum results.

3.3. Site Symmetry of YBO_3:Eu Nanocrystals. *3.3.1. Wavelength-Selected Excitation and Emission Spectra.* The excitation spectra obtained by monitoring the emissions of $^5D_0 \rightarrow {}^7F_1$ (at 591 nm) and $^5D_0 \rightarrow {}^7F_2$ (at 610 nm) for YBO_3:Eu were given in Figure 7. The broad bands showed in the spectra originated from the charge-transfer excitation (CT). For all samples, a small shift of the CT bands could be observed. The CT bands monitored by $^5D_0 \rightarrow {}^7F_1$ were located at a shorter wavelength compared with those of $^5D_0 \rightarrow {}^7F_2$. Figure 8 shows the emission spectra of YBO_3:Eu under different wavelength UV excitation. The $^5D_0 \rightarrow {}^7F_1$ emissions are relatively strong when excited at a relatively short wavelength and become weaker under a longer wavelength excitation. The results indicated that Eu^{3+} ions could be excited preferentially by different excitation sources. There seems to be at least two different luminescent sites existing in YBO_3:Eu, one of which possesses a superior symmetry while the other possesses an inferior symmetry. These two kinds of sites were denoted successively as site **1** and **2**, respectively, in the following description. In comparison with Eu^{3+} ions in site **2**, Eu^{3+} ions in site **1** have a relatively lower intensity ratio of $^5D_0 \rightarrow {}^7F_2$ to $^5D_0 \rightarrow {}^7F_1$ (red/orange or R/O). And the CT band of Eu^{3+} ions in site **1** is located at a relatively shorter wavelength.

As reported by Lin et al.[35] and Hoefdraad,[36] the peak position of CT band is involved in the length of Eu−O bond: the shorter the Eu−O bond is, the shorter the wavelength of the CT band position will be. Therefore, it can be deduced that the average Eu−O bond distance of site **1** is shorter than that of site **2**.

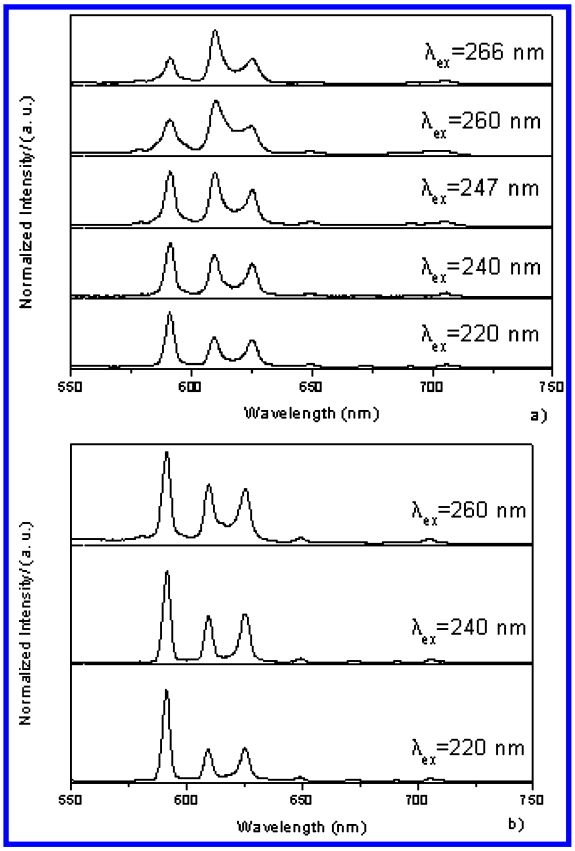

Figure 8. Emission spectra of YBO_3:Eu for (a) sample **b** and (b) bulk under different wavelength UV excitation.

However, it should be noted that the above result does not mean that one can obtain an inferior site symmetry by merely lengthening the Eu−O bond. In this work, we have already pointed out that a relatively larger cell volume can be observed for the YBO_3:Eu samples with smaller particle size or with higher doping concentration. On the basis of these results, it can be considered that the average RE−O bond distance is relatively longer in the YBO_3:Eu samples with smaller particle size and higher doping concentration. However, the former type of Eu−O bond elongating resulted in a superior chromaticity, while the latter one gave an almost unchanged chromaticity. Therefore, inferior site symmetry might be involved in not only the longer Eu−O bond distance but also the more distorted lattices. It is well-known that the interface effects of nanoscaled materials might lengthen the Eu−O bond distance, for example, as was reported by Tao et al.[37] for the Y_2O_3:Eu and Y_2SiO_5:Eu nanocrystals. Also it has been reported that in nanosized materials the degree of disorder is high while the crystal field symmetry is low.[9] Therefore, it should not be unique characteristics of hexagonal YBO_3:Eu system to observe such chromaticity improvement. In fact, if one compares the fluorescence spectrum of the nanoscaled triclinic $GdBO_3$:Eu[38] with that of the bulk triclinic $GdBO_3$:Eu,[39] one can easily find that the chromaticity is also improved in such nanoscaled materials. However, until recently, little attention has been paid to the chromaticity improvement in nanoscaled materials.

3.3.2. Site-Selective Excitation and Emission Spectra. The high-resolution emission spectra of samples **a** and **b** and the bulk were measured under 266 nm UV excitation and displayed in Figure 9a. The three groups of emission peaks between 570 and 640 nm can be attributed to $^5D_0 \rightarrow {}^7F_j$ ($j = 0,1,2$) transitions of Eu^{3+} ions. A larger R/O ratio can be observed for the nanocrystals, which coincides satisfactorily with the above

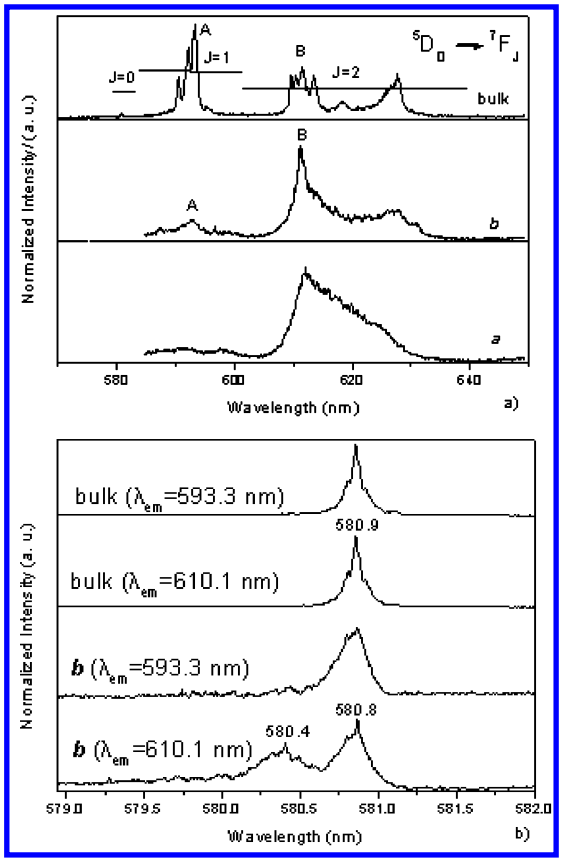

Figure 9. High-resolution emission spectra (a) of YBO_3:Eu for samples **a** and **b** and bulk under 266 nm UV excitation and (b) excitation spectra of lines A (at 593.3 nm) and B (610.1 nm) from panel a.

studies of this work. Only one $^5D_0 \rightarrow {}^7F_0$ transition located at 580.9 nm appeared for the bulk as shown in Figure 9a. The other two groups of emission, which corresponded to $^5D_0 \rightarrow {}^7F_1$ and $^5D_0 \rightarrow {}^7F_2$, are denoted as A (maximum at 593.3 nm) and B (maximum at 610.1 nm). Figure 9b shows the excitation spectra, which are associated with the $^5D_0 \rightarrow {}^7F_0$ of Eu^{3+} ions, of the emission lines A and B in Figure 9a. The excitation spectrum for the nanocrystals (sample **b**) by monitoring line B shows two peaks located at 580.8 and 580.4 nm (by Gaussian fitting), whereas the other excitation spectra only give one peak located at 580.8 and 580.9 nm for the nanocrystals and the bulk, respectively.

Generally, the $^5D_0 \rightarrow {}^7F_0$ transition of Eu^{3+} is a parity-forbidden one, but when Eu^{3+} ions occupy one of the C_s, C_1, C_2, C_3, C_4, C_6, C_{2v}, C_{3v}, C_{4v}, and C_{6v} (i.e., C_s, C_n, C_{nv}) sites, the parity forbiddance will be partially permitted and thus a $^5D_0 \rightarrow {}^7F_0$ emission can be observed.[31] Furthermore, the $^7F_0$ and $^5D_0$ state levels do not split. Therefore, the $^5D_0 \rightarrow {}^7F_0$ transition is commonly utilized to deduce the number of C_s, C_n, and C_{nv} sites in luminescent materials.[40] Based on the above results, two conclusions can be drawn in our case. First, there is only one of C_s, C_n, and C_{nv} sites existing in the bulk, while two of them are present in the nanocrystals. Second, for the excitation spectrum in the nanocrystals by monitoring line B, the peak located at 580.8 nm belongs to Eu^{3+} ions in the intrinsic site of YBO_3:Eu (referred as site **I**) and the peak located at 580.4 nm should be related to Eu^{3+} ions located in the surface site (referred as site **3**). The results are in agreement with the earlier report[40] on the Y_2SiO_5:Eu nanocrystals, in which the excitation spectra showed four $^5D_0 \rightarrow {}^7F_0$ lines and the authors attribute the forth line to a surface site. Similarly, the phenomenon that one crystalline site and one disordered site are presented in the

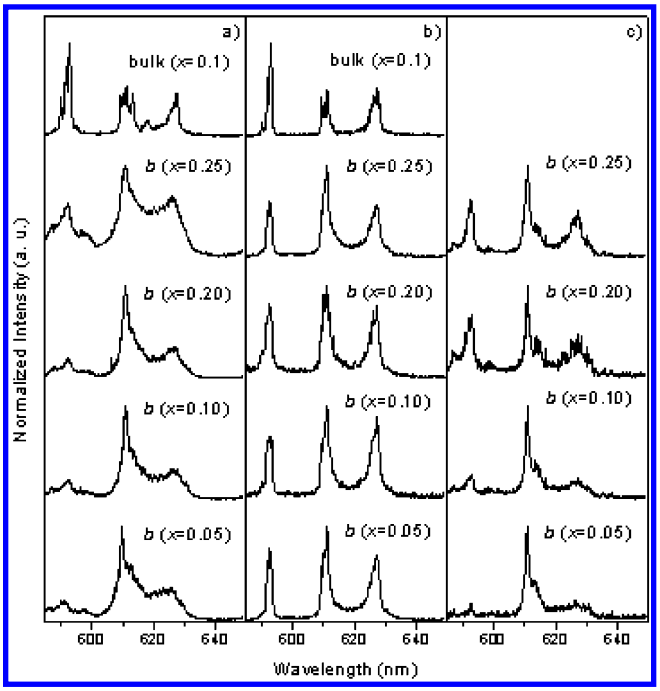

Figure 10. Emission spectra of $Y_{1-x}BO_3$:Eu_x for **b** series samples and bulk under (a) 266 nm UV excitation and by exciting (b) site **1** and (c) site **3**.

nanocrystals is also observed by other authors even earlier. However, those reports did not mention what is the physical relationship of these two types of sites.[12]

In Figure 9b, the two spectrum peaks of the nanocrystals are both located at shorter wavelength region compared with that of the bulk. The small blue shift can be interpreted by the nephelauxetic effect of RE ions[31] on the basis of the above cell volume data. The theory about the nephelauxetic effect of RE ions states that in crystal field the 4f orbitals of RE ions are expanded and mixed with the opposite parity 5d orbitals and thus are concerned with bonding. The nephelauxetic effect causes the decrease of electron−electron repellence in RE ions and corresponding decrease of 4f level gap in RE ions, and as a result, spectrum lines of RE ions shift to a longer wavelength (red shift) in comparison with the corresponding spectrum lines of RE atoms. In our case, in comparison with the bulk, the nanocrystals possess a relatively weaker crystal field because of the larger cell volume. The nephelauxetic effect of Eu^{3+} ions correspondingly becomes weaker in the nanocrystals, which should be responsible for the blue shift of the $^5D_0 \rightarrow {}^7F_0$ excitation lines. Furthermore, it can be deduced that the cell volume of the site **3** is relatively larger compared with that of site **1**. The blue shift of the $^5D_J \rightarrow {}^7F_J$ transition in nanocrystals is ubiquitous, as observed in cubic Y_2O_3:Eu[41] and monoclinic Y_2O_3:Eu.[11−14] However, only a few authors[41] attributed the blue shift to the nephelauxetic effect of Eu^{3+} ions.

Site-selectively excited emission spectra were recorded under pumping at 580.4 and 580.8 nm for the nanocrystals (sample **b** for different Eu^{3+} concentration) and at 580.9 nm for the bulk. The emission spectra belong to site **1** were shown in Figure 10b, and those belonging to site **3** were shown in Figure 10c. To compare with the site-selectively excited emission spectra, the unselected excitation luminescence spectra were presented in Figure 10a. Compared with Figure 10a, some lines vanished and other lines presented relatively lower intensities in Figure 10b, suggesting the existence of another site, which coincides with the above analyses (see section 3.3.1). Moreover, three emission peaks of $^5D_0 \rightarrow {}^7F_1$ transition and five emission peaks

of $^5D_0 \rightarrow {}^7F_2$ transition can be observed. The results meant that the ground states $^7F_1$ and $^7F_2$ split into three and five levels, respectively; therefore, we considered that Eu^{3+} ions in site **1** are in C_1 symmetry coordination.[42] The assignment of the site **1** is in agreement with the reports of Lin et al.[6]

In Figure 10b,c, as far as the R/O value is concerned, the luminescent spectra of the nanocrystals evidently differ from that of the bulk. The R/O values in the nanocrystals are greater than 1, whereas it is less than 1 for the bulk. It is prominent that both site **1** and **3** should be responsible for the superior chromaticity in the nanocrystals. However, for the same nanocrystals (sample **b**), spectra with a R/O value greater than 1 have already been presented in section 3.3.1 under 240 and 220 nm UV excitation. Hereby, there must be another site, and the spectrum R/O value of Eu^{3+} in this site should be greater than 1, which means this site should have a relatively lower symmetry in comparison with sites **1** and **3**. Therefore, site **1** in the above discussion is just site **2** in section 3.3.1.

Moreover, when Eu^{3+} concentration was equal to or greater than the quenching concentration ($x = 0.20$), the R/O values belonging to site **2** became lower while those of site **3** became higher, suggesting a pronounced energy transfer between site **2** and site **3** in the nanocrystals. As mentioned above, in earlier studies, there was a pendent question about what is the physical relationship of the two sites in nanocrystals (one crystalline site and one disordered site).[9−14] Some authors considered that these two sites could exist as a disordered surface site surrounding a crystalline interior, while other authors considered that they result from the distribution of particle size, the larger particles producing the crystalline spectra and the smaller particles producing the disordered spectra. It is generally accepted that there are no ion−ion interactions across the particle interface.[12,13,33] On the basis of this, it can be deduced that if the latter opinion was true, then no energy transfer would occur between these two sites. Therefore, site **3** must be a surface site surrounding the interior site, site **2**. Owing to the long distance between the luminescent centers in site **2** and those in site **3**, one can deduce that the energy transfer between these two sites should be very weak before the resonant energy transfer net of luminescent centers was formed. In Figure 10, when Eu^{3+} concentration was lower than the quenching concentration, that is, before the resonant energy transfer net of luminescent centers was not formed, the energy transfer was certainly very weak.

It is well-known that the energy transfer strongly depends on the temperature and the energy mismatch.[40,43] The $^5D_0$ level of Eu^{3+} ions in site **2** is located at a lower energy region compared with that in site **3**, and the mismatch is an energy difference $|\Delta E_{23}| = 12\ cm^{-1}$. Therefore, the relative transfer rates can be described as[40,43]

$$(w_{3\rightarrow 2})/(w_{2\rightarrow 3}) = [n(|\Delta E_{23}|) + 1]/[n(|\Delta E_{23}|)] = \exp(|\Delta E_{23}|/(kT))$$

At room temperature (300 K), $(|\Delta E_{23}|)/(kT) = 12/208.5$ and $(w_{3\rightarrow 2})/(w_{2\rightarrow 3}) \approx 1.06$. The transfer rate from site **3** to **2** is almost equal to but slightly higher than that from site **2** to **3**. Consequently, the two emission spectra are similar to each other after the resonant energy transfer net of luminescent centers was formed.

Figure 11 shows the temporal behaviors of the $^5D_0 \rightarrow {}^7F_2$ emission after respective site **2** and **3** selective excitation. Results showed that when Eu^{3+} concentration was greater than the quenching concentration, the lifetimes of site **2** and **3** both

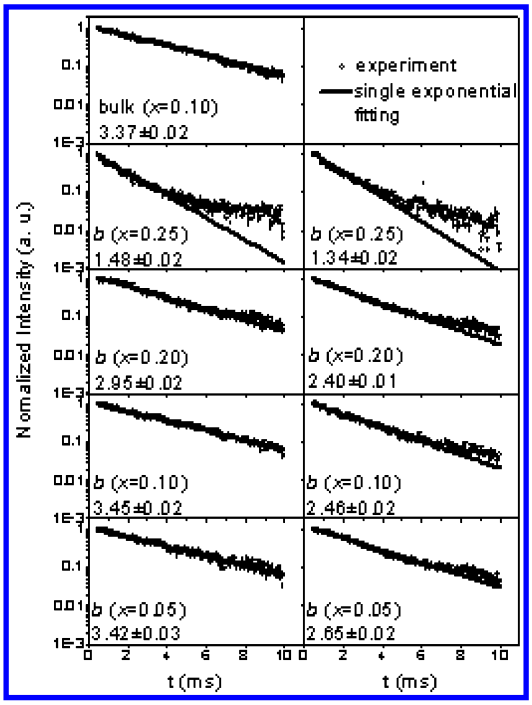

Figure 11. Decay curves of the $^5D_0 \rightarrow {}^7F_2$ emission by exciting (left) site **2** and (right) site **3**.

became relatively shorter and had a great deviation from single exponent. Such phenomenon may result from the energy transfer between site **2** and **3**, as evident in Figure 10. For $x = 0.10$ samples, the nanocrystals exhibit a relatively longer lifetime in site **2** while a relatively shorter lifetime in site **3** compared with the bulk. In previous studies, Schmechel et al.[44] and Tissue et al.[12,14] considered that Y_2O_3:Eu nanocrystals possessed relatively longer lifetimes than the bulk; they attributed their results to the decrease of the radiative transition rates in nanocrystals, while in the contrary, Huang et al.[45] observed relatively shorter lifetimes in the nanocrystals, and they attribute the shortening to the energy transfer from a surface site. On the basis of our results, we considered that both deductions were reliable, although they were formally different. If the energy transfer from the surface to the interior was effective, the latter one should be dominant, and then a relatively shorter lifetime could be perceived. To the opposite, if the energy transfer from the surface to the interior was ineffective, the former one should be turned into the deciding factor, and thus a relatively longer lifetime could be observed. In such studies, because of different fabrication methods, the energy transfer from the surface to the interior should exhibit different behavior.

Moreover, one can clearly discover that the lifetime of the $Y_{1-x}BO_3$:Eu_x nanocrystals at its quenching concentrations ($x = 0.20$) is shorter than that of the bulk ($x = 0.08$) from Figure 11. Because the decay time of bulk YBO_3:Eu is somewhat longer for practical application,[2] the short lifetime of the nanocrystals should be of benefit to its utilizations.

4. Conclusions

Pure hexagonal-phased YBO_3:Eu nanocrystals with different particle sizes were prepared by a convenient sol−gel pyrolysis process, and their photoluminescence spectra showed the size-dependent chromaticity, that, the R/O ratio was much higher in the smaller sized samples. Both XRD patterns and IR spectra exhibited that the lattices of YBO_3:Eu nanocrystals were distorted, and as the particle size became smaller, the lattices became more distorted. Studies on the CT bands indicated that

Eu^{3+} ions can be excited preferentially by different excitation sources in both the bulk and nanocrystals, which suggested that at least two different intrinsic luminescent sites, site **1** and site **2**, coexisted in YBO_3:Eu. Site **2**, the site with relatively inferior symmetry, was clarified to be of C_1 symmetry. Site-selective excitation spectra also present a particular site, site **3**, in the nanocrystals. For the nanocrystals, Eu^{3+} ions in both site **2** and site **3** displayed improved R/O values, which might be resulted from the distorted lattices and should be responsible for the superior chromaticity. A pronounced energy transfer between site **2** and site **3** in the nanocrystals was observed, while the doping concentration was higher than the quenching concentration, which indicated that site **3** may be a disordered surface site surrounding the interior sites. At quenching concentrations, the lifetime of the nanocrystals is shorter than that of the bulk and the luminescent intensity of the nanocrystals is higher than that of the bulk. On the basis of its superior chromaticity, relatively shorter lifetime, and higher luminescent intensity, the YBO_3:Eu nanocrystal is considered to be a promising VUV phosphor.

Acknowledgment. This work is supported by the NSFC (Grants 20001002, 20013005), MOST (Grant G19980613), MOE (the Foundation for University Key Teacher), and the Founder Foundation of PKU.

References and Notes

(1) Ronda, C. R.; Jüstel, T.; Nikol, H. *J. Alloys Compd.* **1998**, *275*−*277*, 669.
(2) Kim, C. H.; Kwon, I. E.; Park, C. H.; Hwang, Y. J.; Bae, H. S.; Yu, B. Y.; Pyun, C. H.; Hong, G. Y. *J. Alloys Compd.* **2000**, *311*, 33.
(3) Wegh, R. T.; Donker, H.; Oskam, K. D.; Meijerink, A. *Science* **1999**, *283*, 663.
(4) Wegh, R. T.; Donker, H.; Van Loef, E. V. D.; Oskam, K. D.; Meijerink, A. *J. Lumin.* **2000**, *87*−*89*, 1017.
(5) Feldmann, C.; Jüstel, T.; Ronda, C. R.; Wiechert, D. U. *J. Lumin.* **2001**, *92*, 245.
(6) Ren, M.; Lin, J. H.; Dong, Y.; Yang, L. Q.; Su, M. Z.; You, L. P. *Chem. Mater.* **1999**, *11*, 1576.
(7) Yang, Z.; Ren, M.; Lin, J. H.; Su, M. Z.; Tao, Y.; Wang, W. *Chem. J. Chin. Univ.* **2000**, *21*, 1339.
(8) Wei, Z. G.; Sun L. D.; Liao, C. S.; Yan, C. H.; Huang, S. H. *Appl. Phys. Lett.* **2002**, *80*, 1447.
(9) Tao, Y.; Zhao, G. W.; Zhang, W. P.; Xia, S. D. *Mater. Res. Bull.* **1997**, *32*, 501.
(10) Li, Q.; Gao, L.; Yan, D. S. *Chem. Mater.* **1999**, *11*, 533.
(11) Williams, D. K.; Bihari, B.; Tissue, B. M.; McHale, J. M. *J. Phys. Chem. B* **1998**, *102*, 916.
(12) Tissue, B. M. *Chem. Mater.* **1998**, *10*, 2837.
(13) Tissue, B. M.; Bihari, B. *J. Fluoresc.* **1998**, *8*, 289.
(14) Eliers, H.; Tissue, B. M. *Chem. Phys. Lett.* **1996**, *251*, 74.
(15) Holsä, J. *Inorg. Chim. Acta* **1987**, *139*, 257.
(16) Chadeyron, G.; Mahiou, R.; El-Ghozzi, M.; Arbus, A.; Zambon, D.; Cousseins, J. C. *J. Lumin.* **1997**, *72*−*74*, 564.
(17) Newnham, R. E.; Redman, M. J.; Santoro, R. P. *J. Am. Ceram. Soc.* **1963**, *46*, 253.
(18) Bradley, W. F.; Graf, D. L.; Roth, R. S. *Acta Crystallogr.* **1966**, *20*, 283.
(19) Zhang, W. W.; Xie, P. B.; Zhang, W. P.; Yin, M.; Jing, L.; Lü, S. Z.; Lou, L. R.; Xia, S. D. *J. Inorg. Mater.* **2001**, *16*, 9.
(20) Boyer, D.; Bertrand-Chadeyron, G.; Mahiou, R.; Caperaa, C.; Cousseins, J. C. *J. Mater. Chem.* **1999**, *9*, 211.
(21) Li, Y. Y.; Peng, M. L.; Feng, S. H. *Chin. Chem. Lett.* **1996**, *7*, 387.
(22) Kim, D. S.; Lee, R. Y. *J. Mater. Sci.* **2000**, *35*, 4777.
(23) Lou, L.; Boyer, D.; Bertrand-Chadeyron, G.; Bernstein, E.; Mahiou, R.; Mugnier, J. *Opt. Mater.* **2000**, *15*, 1.
(24) Kustin, K.; Pizer, R. *J. Am. Chem. Soc.* **1969**, *91*, 317.
(25) Langford, J. I. *J. Appl. Crystallogr.* **1973**, *6*, 190.
(26) Denning, J. H.; Ross, S. D. *Spectrochim. Acta* **1972**, *28A*, 1775.
(27) Laperches, J. P.; Tarte, P. *Spectrochim. Acta* **1966**, *22*, 1201.
(28) Skoog, D. A.; West, D. M. *Principal of Instrumental Analysis*, 2nd ed.; Saunders College: Philadephia, PA, 1980.
(29) Huignard, A.; Gacoin, T.; Pierre, J. P. *Chem. Mater.* **2000**, *12*, 1090.
(30) Riwotzki, K.; Haase, M. *J. Phys. Chem. B* **1998**, *102*, 10129.
(31) Reisfeld, R.; Jörgensen, C. K. *Lasers and Excited States of Rare Earths*; Springer-Verlag: Berlin, Heidelberg, 1977.
(32) Sun, L. D.; Yao, J.; Liao, C. S.; Yan, C. H. *Physics and Chemistry of Nanostructured Materials*; Taylor & Francis Inc.: New York, 1999; p 188.
(33) Zhang, W. P.; Xie, P. B.; Duan, C. K.; Yan, K.; Yin, M.; Lou, L. R.; Xia, S. D.; Krupa, J. C. *Chem. Phys. Lett.* **1998**, *292*, 133.
(34) Dhanaraj, J.; Jagannathan, R.; Kutty, T. R. N.; Lu, C. H. *J. Phys. Chem. B* **2001**, *105*, 11098.
(35) Lin, J. H.; You, L. P.; Lu, G. X.; Yang, L. Q.; Su, M. Z. *J. Mater. Chem.* **1998**, *8*, 1051.
(36) Hoefdraad, H. E. *J. Solid State Chem.* **1975**, *15*, 175.
(37) Tao, Y.; Zhao, G. W.; Ju, X.; Shao, X. G.; Zhang, W. P.; Xia, S. D. *Mater. Lett.* **1996**, *28*, 17.
(38) Zhang, W. W.; Xie, P. B.; Zhang, W. P.; Yin, M.; Lou, L. R.; Xia, S. D. *J. Inorg. Mater.* **2001**, *16*, 470.
(39) Corbel, G.; Leblanc, M.; Antic-Fidancev, E.; Lemaitre-Blaise, M.; Krupa, J. C. *J. Alloys Compd.* **1999**, *287*, 71.
(40) Yin, M.; Duan, C.; Zhang, W.; Lou, L.; Xia, S.; Krupa, J. C. *J. Appl. Phys.* **1999**, *86*, 3751.
(41) Zhang, W. W. Ph.D. Thesis, University of Science and Technology of China, Hefei, China, 2001.
(42) Reid, M. F.; Richardson, F. S. *J. Chem. Phys.* **1983**, *79*, 5735.
(43) Yin, M.; Corbel, G.; Leblanc, M.; Antic-Fidancev, E.; Krupa, J. C. *J. Alloys Compd.* **2000**, *302*, 12.
(44) Schmechel, R.; Kennedy, M.; Von Seggern, H.; Winkler, H.; Kolbe, M.; Fischer, R. A.; Li, X.; Benker, A.; Winterer, M.; Hahn, H. *J. Appl. Phys.* **2001**, *89*, 1679.
(45) Li, D.; Lü, S. Z.; Chen, B. J.; Wang, H. Y.; Tang, B.; Zhang, J. H.; Hou, S. G.; Huang, S. H. *Acta Phys. Sin.* **2001**, *50*, 933.